https://doi.org/10.5194/egusphere-2026-3241
Preprint. Discussion started: 13 July 2026

Anthropogenic CO_2 Emissions in China Constrained by OCO-2/3 XCO_2 Observations

Shenpeng Qiu[1], Shuzhuang Feng[1,2*], Fei Jiang[1,2], Chong Wei[3], Yusheng Shi[4], Mengwei Jia[1,2], Honglin Zhuang[1], Hengmao Wang[1,2], Yongguang Zhang[1,2], Weimin Ju[1,2]

[1]Jiangsu Provincial Key Laboratory for Advanced Remote Sensing and Geographic Information Technology, International Institute for Earth System Science, Nanjing University, Nanjing, 210023, China

[2]Jiangsu Center for Collaborative Innovation in Geographical Information Resource Development and Application, Nanjing, 210023, China

[3]Shanghai Carbon Data Research Center, CAS Key Laboratory of Low-Carbon Conversion Science and Engineering, Shanghai Advanced Research Institute, Chinese Academy of Sciences, Shanghai, 201210, China

[4]State Key Laboratory of Remote Sensing Science, Aerospace Information Research Institute, Chinese Academy of Sciences, Beijing, 100101, China

* Corresponding author: Prof. Shuzhuang Feng (fengsz@nju.edu.cn)

https://doi.org/10.5194/egusphere-2026-3241
Preprint. Discussion started: 13 July 2026

Abstract: Accurately quantifying anthropogenic CO_2 emissions is essential for evaluating carbon budget and mitigation strategies. However, traditional "bottom-up" emission inventories suffer from substantial uncertainties and update time lags, urgently requiring top-down constraints from atmospheric observations while accounting for confounding terrestrial biogenic interferences. In this study, we extended RegGCAS, a regional carbon assimilation system based on the WRF-CMAQ atmospheric chemical transport model and the Ensemble Kalman Filter algorithm. By assimilating column-averaged dry-air CO_2 mole fractions (XCO_2) from OCO-2/3 satellite observations, we inverted anthropogenic CO_2 emissions over mainland China during winter 2022-2023. The results revealed that the total national anthropogenic CO_2 emissions amounted to 2808.3 ± 157.0 Tg, 16.1% higher than the MEIC inventory. For key emission regions, emissions increased by 13.1% in the Beijing-Tianjin-Hebei region, whereas they decreased by 10.4% in the Yangtze River Delta. The system captured distinct urban-suburban emission adjustment differences in key regions, with reductions in city centers and increases in surrounding areas. It also reflected short-term emission fluctuations related to anthropogenic activity changes, such as the Spring Festival work stoppages. Evaluation demonstrates that assimilation effectively reduces prior emission errors by 68.0%. Validation shows that posterior simulation RMSE decrease by 5.8% against the assimilated OCO-2/3 XCO_2, and by 15.3%, 7.7%, and 25.2% against independent TCCON, ObsPack, and urban site observations, respectively, confirming the enhanced accuracy of the posterior emission estimates. This study provides a reliable inversion framework for tracking regional carbon dynamics and refining bottom-up emission inventories.

Keywords: Anthropogenic CO_2 emissions; Emission inversion; OCO-2/3; Data assimilation; RegGCAS

1. Introduction

Atmospheric CO_2 concentrations have increased by approximately 53.2% relative to preindustrial levels, reaching 426.5 ppm in 2025 (WMO, 2025). Anthropogenic CO_2 emissions, primarily from fossil fuel combustion and industrial processes, are the dominant driver of the observed rise in atmospheric CO_2 (Friedlingstein et al., 2024). As the world's largest emitter of anthropogenic CO_2, China urgently needs a scientific, high-spatiotemporal-resolution carbon emission accounting system to achieve its carbon peaking and carbon neutrality goals.

https://doi.org/10.5194/egusphere-2026-3241
Preprint. Discussion started: 13 July 2026

At present, the quantification of anthropogenic CO_2 emissions mainly relies on the "bottom-up" emission inventory approach and the "top-down" atmospheric inversion method (Janssens-Maenhout et al., 2020). The former, based on energy activity levels, emission factors, and statistical data, serves as the fundamental method for current emission estimation (IPCC, 2019). However, its estimates are highly susceptible to factors such as statistical data quality, time lags in updates, and spatial disaggregation methods (Hua et al., 2023; Zhang et al., 2022), leading to uncertainties that can reach up to 50% at the provincial scale in China (Yang et al., 2025). In contrast, the "top-down" approach combines prior emissions, CO_2 observations, and atmospheric transport models to constrain surface emission fluxes through inversion or data assimilation, gradually becoming an essential means for the independent evaluation and correction of emission inventories (Friedlingstein et al., 2024).

In recent years, observation-constrained inversion studies of anthropogenic CO_2 emissions have steadily advanced. Early studies primarily focused on major point sources, such as power plants, as well as high-emission regions including industrial clusters and urban hotspots (Zheng et al., 2020). Since emissions in these areas are highly concentrated, they produce distinct downwind XCO_2 enhancement signals in satellite or airborne measurements, facilitating the estimation of emission intensities when combined with wind field data and plume spatial characteristics (Nassar et al., 2021; Guo et al., 2023; Fuentes Andrade et al., 2024).With the development of observational data and atmospheric transport models (e.g., Lagrangian or Eulerian models), related research has further expanded from specific major sources to the regional scale. Recent studies have utilized satellite XCO_2 observations or ground-based CO_2 measurements to constrain fossil fuel CO_2 emissions in major high-emission urban regions. For example, Lei et al. (2021) used OCO-2 XCO_2 observations and a multi-model approach to estimate fossil fuel CO_2 emissions over Lahore, Pakistan, finding that ODIAC likely underestimates local emissions and that robust urban emission trends require more high-quality satellite overpasses. Lian et al. (2023) used continuous ground-based CO_2 observations and a Bayesian inversion to estimate city-scale CO_2 emissions in the Paris metropolitan area, finding that annual emissions declined across the region from 2016 to 2021. However, compared to inversions targeting point sources, large-regional-scale emission inversions remain relatively scarce (Chevallier and Broquet, 2025), and are predominantly focused on quantifying biogenic carbon fluxes (Zhang et al., 2024a). At the regional scale, inversions of anthropogenic CO_2 emissions are susceptible to the combined effects of biogenic carbon

https://doi.org/10.5194/egusphere-2026-3241
Preprint. Discussion started: 13 July 2026

fluxes and variations in background CO_2 concentrations (Oney et al., 2017; Schuh et al., 2019). Consequently, effectively separating the anthropogenic emission signals from these interferences remains a critical challenge.

Given the common sources of air pollutants and CO_2, some studies have indirectly estimated anthropogenic CO_2 emissions by using observations to invert co-emitted species related to fossil fuel combustion, such as NO_X or CO, and then combining them with CO_2-to-NO_X or CO_2-to-CO emission ratios from prior inventories (Li et al., 2025; Konovalov et al., 2016). For example, Feng et al. (2024) utilized surface NO_2 observations to invert fossil fuel CO_2 emissions in China, finding that "bottom-up" emission inventories generally underestimate carbon emissions from the energy and power sectors in western China, while significantly overestimating them in developed regions and key urban areas. Owing to the relatively high observational coverage of proxy gases, this approach presents distinct advantages in regional emission studies, as it can provide supplementary constraints when direct CO_2 observations are insufficient. However, the estimates remain sensitive to uncertainties and time lags in the emission ratios from bottom-up inventories (Juchem et al., 2025).

During winter, biogenic carbon fluxes, wildfire carbon emissions, and ocean carbon fluxes are significantly weaker than anthropogenic emissions. Taking the Yangtze River Delta (YRD) as an example, biogenic sources accounted for only 0.2% of anthropogenic emissions during winter (Zhang et al., 2024b). Therefore, winter is a more suitable period for inverting anthropogenic CO_2 emissions to minimize interference from natural source signals. Based on a regional carbon assimilation system RegGCAS (Feng et al., 2025), Zhang et al. (2024b) inverted anthropogenic CO_2 emissions in the YRD during winter by assimilating ground-based CO_2 observations. This approach can effectively reduce prior emission uncertainties and has considerable application potential. However, as ground-based CO_2 observations are sparsely distributed across only a few specific cities, it remains challenging to provide effective constraints on anthropogenic emissions at the national scale.

Given the sparse ground-based observations and biogenic signal interference in regional anthropogenic CO_2 inversion, this study integrates OCO-2/3 XCO_2 observations into RegGCAS to invert national anthropogenic CO_2 emissions during winter 2022-2023. This work advances previous RegGCAS applications by expanding the observational constraints from sparse ground-based data to satellite XCO_2, widening the inversion scope from the regional YRD to the national scale, and transitioning from a single-source

https://doi.org/10.5194/egusphere-2026-3241
Preprint. Discussion started: 13 July 2026

optimization to a joint inversion of both anthropogenic and biogenic fluxes. The robustness and reliability of the inversion are further evaluated using an Observing System Simulation Experiment (OSSE), independent observations, and sensitivity experiments.

2. Data and Methods

2.1 Data assimilation system

RegGCAS is a regional carbon assimilation system developed as an extension of the Regional multi-Air Pollutant Assimilation System (RAPAS) (Feng et al., 2023). Previous work with this system has already assimilated ground-based CO_2 observations to optimize anthropogenic CO_2 emissions (Zhang et al., 2024b) and TROPOMI observations to constrain CH_4 emissions (Feng et al., 2025). This study further expanded RegGCAS by incorporating OCO-2/3 XCO_2 observations to optimize regional anthropogenic CO_2 emissions. The system comprises a regional chemical transport model (WRF-CMAQ) and an ensemble Kalman filter (EnKF) data assimilation module, used respectively to simulate the spatiotemporal distribution of atmospheric CO_2 and to update anthropogenic emissions under observational constraints. Within each data assimilation window, RegGCAS adopted a "two-step" inversion scheme. In the forecast step, CMAQ simulated the CO_2 concentration field based on prior emissions, establishing the response relationship between emissions and satellite XCO_2 observations. Subsequently, in the analysis step, satellite XCO_2 observations were used to optimize the prior emissions and obtain posterior emissions. These updated emissions were then passed as the prior emissions for the next window, further driving CMAQ to generate the initial concentration field for that window. This scheme enables observational information to be propagated across adjacent windows, allowing iterative updates of emissions and thereby improving inversion accuracy and stability (Feng et al., 2024).

2.1.1 Atmospheric transport model

In this study, the Weather Research and Forecasting (WRF v4.0) model (Skamarock and Klemp, 2008) and the Community Multiscale Air Quality (CMAQ v5.0.2) model (Byun and Schere, 2006) were employed to simulate the meteorological fields and CO_2 transport processes, respectively. The CMAQ modeling domain covers mainland China and its surrounding regions (Fig. 1a), with a horizontal resolution of 27 km and 225 × 165 grid

https://doi.org/10.5194/egusphere-2026-3241
Preprint. Discussion started: 13 July 2026

cells. Vertically, 25 sigma-pressure layers were set from the surface up to 100 Pa. To better characterize the urban underlying surface, the MODIS land cover product (MCD12C1, version 6.1) for 2022 was used to update the urban and built-up land information in the model. Meteorological initial and lateral boundary conditions for WRF were derived from the National Centers for Environmental Prediction Final Analysis (NCEP FNL) data at 1° × 1° resolution and 6 h intervals. The initial field for the first assimilation window and the lateral boundary conditions were both derived from the inversion-optimized results of the Global Carbon Assimilation System (GCAS) v2 (Jiang et al., 2021). Considering that CO_2 is a long-lived gas and chemically inert over the study period, gas-phase chemistry and aerosol-related processes were disabled in CMAQ, retaining only physical processes (e.g., transport and diffusion). This configuration allows the simultaneous simulation of CO_2 concentration ensembles while reducing computational cost.

2.1.2 EnKF assimilation algorithm

The ensemble Kalman filter (EnKF) employs a Monte Carlo approach, using a set of ensemble states to represent the probability distribution of the true state (Evensen, 2003). Through the assimilation of observations, the model states are updated iteratively, minimizing the deviation between simulations and observations. In this study, the Ensemble Square Root Filter (EnSRF) method was used to optimize anthropogenic CO_2 emissions (Whitaker and Hamill, 2002).

The EnSRF first applied a zero-mean Gaussian perturbation to the background state vector X^b to construct an ensemble of model states, with the perturbation magnitude determined by the state uncertainty. Subsequently, the background error covariance matrix P^b was calculated based on these ensemble samples:

$$P^b = \frac{1}{N-1}\sum_{i=1}^{N}\left(X_i^b - \overline{X^b}\right)\left(X_i^b - \overline{X^b}\right)^T \tag{1}$$

where N is the ensemble size; X_i^b represents the ith ensemble sample; and $\overline{X^b}$ is the ensemble mean. The background error covariance matrix P^b was used to represent the uncertainty of the background field and its error correlation structure, providing the basis for subsequent state updates. In the forecast step, WRF-CMAQ advanced each ensemble member to the next time step, propagating the emission perturbations to the CO_2 concentration field, thereby establishing the response relationship between concentrations

https://doi.org/10.5194/egusphere-2026-3241
Preprint. Discussion started: 13 July 2026

and emissions. In the analysis step, the observation vector y was further introduced to update the background state, yielding the analyzed state ensemble mean $\overline{X^a}$, which was taken as the optimal estimate of the emissions at the current time:

$$\overline{X^a} = \overline{X^b} + K\left(y - H\overline{X^b}\right) \quad (2)$$

$$K = P^b H^T (HP^b H^T + R)^{-1} \quad (3)$$

where R is the observation error covariance matrix; and K is the Kalman gain matrix that determines the relative weights of background and observational information.

OCO-2/3 provides XCO_2, whereas the model outputs three-dimensional CO_2 concentrations. Therefore, an observation operator H is required to map the model state into the satellite observation space. Specifically, the CO_2 vertical profile of the corresponding grid was first extracted from CMAQ based on the latitude, longitude, and time of the observation. The model-layer concentrations were then interpolated to the OCO retrieval layers using pressure-level information, yielding a simulated profile x_i^m consistent with the satellite vertical layering. On this basis, the simulated XCO_2 was calculated as follows:

$$XCO_2^m = XCO_2^a + \sum_{i=1}^{n} w_i A_i (x_i^m - x_i^a) \quad (4)$$

where XCO_2^m is the simulated XCO_2 processed by the observation operator; XCO_2^a is the prior XCO_2 from the satellite product; x_i^m and x_i^a denote the modeled CO_2 concentration and satellite prior profile at the ith retrieval layer, respectively; A_i and w_i represent the averaging kernel and pressure weight for that layer; and n is the number of satellite retrieval layers.

The system used 50 ensemble members and a 3-day assimilation window. This is because it takes time for emission perturbations to propagate to the concentration field. Appropriately extending the window allows more satellite observations to be incorporated, thereby enhancing the constraints on emissions. However, if the window is set too long, transport errors and spurious correlations within the ensemble filter will gradually accumulate, which may degrade the assimilation performance (Feng et al., 2023). Furthermore, to address the problem of spurious long-distance correlations in the EnKF (Houtekamer and Mitchell, 2001), this study applied covariance localization using the Gaspari-Cohn localization function (Gaspari and Cohn, 1999). This function is a piecewise continuous fifth-order polynomial approximation of a normal distribution (Miyazaki et al., 2017), allowing the covariance to decrease gradually with distance and thereby reducing the unreasonable influence of remote observations on local analyses. Taking into account the ensemble size, the data assimilation window length, and the transport characteristics of CO_2, the localization scale was set to 500 km (Flowerdew, 2015).

2.2 Prior emissions

In the initial data assimilation window, prior anthropogenic CO_2 emissions were prescribed using the Multi-resolution Emission Inventory for China (MEIC) v1.4 2019 inventory (Fig. 1a) for mainland China (Li et al., 2017a) and the MIX Asian anthropogenic emission inventory for other regions (Li et al., 2017b). In each subsequent window, the prior anthropogenic CO_2 emissions were set to the posterior emissions from the previous window and updated progressively, so that the sensitivity to errors in the original inventory gradually decreased. To mitigate the interference of terrestrial biosphere fluxes on anthropogenic emission estimates, biogenic carbon fluxes were integrated into the assimilation system for joint optimization. Prior biogenic carbon fluxes were derived from the net ecosystem production (NEP) simulated by the Boreal Ecosystem Productivity Simulator (BEPS) model (Wang et al., 2021) at $0.073^{\circ} \times 0.073^{\circ}$ resolution. Prior uncertainties for anthropogenic emissions and biogenic fluxes were assigned grid-cell values of 40% and 80%, respectively, accounting for the errors from statistical data, spatial disaggregation, and biophysical modeling (Super et al., 2024). Additionally, the system incorporated biomass burning emissions and ocean carbon fluxes to represent regional-scale CO_2 background variations. Specifically, fire carbon emissions were taken from the Global Fire Emissions Database (GFED) v4.1s (Randerson et al., 2017) at $0.25^{\circ} \times 0.25^{\circ}$ and 3-hour resolution. Ocean carbon fluxes were obtained from the simulations of GCAS v2 (Jiang et al., 2021) at $1^{\circ} \times 1^{\circ}$ and 3-hour resolution.

2.3 Observation data

This study assimilated bias-corrected Level 2 Lite XCO_2 retrievals from OCO-2 v11.2r and OCO-3 v10.4r, both processed with the Atmospheric Carbon Observations from Space (ACOS) algorithm. OCO-2 operates in a sun-synchronous polar orbit, providing regular global coverage, whereas OCO-3, mounted on the International Space Station, provides more flexible observing modes, including target and Snapshot Area Map observations. Consequently, the two missions differ in spatial coverage, overpass time, viewing geometry,

https://doi.org/10.5194/egusphere-2026-3241
Preprint. Discussion started: 13 July 2026

and data density (Eldering et al., 2019). Despite these sampling differences, quality-filtered and bias-corrected XCO_2 retrievals from OCO-2 and OCO-3 are broadly consistent. (Taylor et al., 2023) reported a mean difference of 0.2 ppm over land between collocated OCO-3 and OCO-2 observations, indicating negligible systematic biases. Thus, combining OCO-2 and OCO-3 XCO_2 data increases observational coverage and strengthens constraints for regional-scale CO_2 emission inversions.

During preprocessing, we retained only Land Nadir and Land Glint (LNLG) observations to match the terrestrial inversion domain and reduce retrieval uncertainties over non-land surfaces. Invalid or missing XCO_2 values were removed, and only high-quality retrievals (xco2_quality_flag = 0) were used to mitigate the influence of clouds, aerosols, and instrument noise. The spatial distribution and counts of the assimilated observations are shown in Fig. 3. For the EnSRF assimilation, the XCO_2 uncertainty from the satellite products was used as the observation error for each observation.

2.4 Evaluation method and data

To evaluate the performance of the RegGCAS and the accuracy of the posterior anthropogenic CO_2 emissions, this study conducted analyses from two aspects: the consistency evaluation using assimilated observations and validation using independent observations (Bocquet et al., 2015). The consistency evaluation used OCO-2/3 XCO_2 observations to compare the agreement between the model simulations (before and after assimilation) and the assimilated observations, thereby testing the internal consistency of the assimilation system (Whitaker and Hamill, 2002). For independent validation, we used non-assimilated ground-based CO_2 observations from public observational networks and an additional urban observation site. The public datasets included XCO_2 observations from the Total Carbon Column Observing Network (TCCON) at Xianghe (XH) and Hefei (HF), and CO_2 concentrations from the ObsPack GLOBALVIEWplus v10.1 dataset at five sites: DSI, LLN, TAP, AMY, and WLG. In addition, in situ CO_2 observations from the Shanghai Zhangjiang urban site (ZJ; 31.18°N, 121.59°E), measured by a Picarro G2301 cavity ring-down spectrometer, were used to further evaluate posterior CO_2 simulations over the YRD urban region. Located on the rooftop of the Shanghai Advanced Research Institute, Chinese Academy of Sciences, in Zhangjiang Hi-Tech Park, this site is surrounded by educational and commercial districts and lies near urban expressways, thus providing a critical assessment of a region with intense anthropogenic activity. Together, these observations

https://doi.org/10.5194/egusphere-2026-3241
Preprint. Discussion started: 13 July 2026

provided independent constraints on the simulated atmospheric CO_2 from both column and near-surface perspectives. The spatial distribution of all validation sites is shown in Fig. 2a. The evaluation metrics included mean bias (BIAS), mean absolute error (MAE), root mean square error (RMSE), and correlation coefficient (CORR).

To corroborate the emission adjustments derived from OCO-2/3 XCO_2 assimilation, this study additionally employed a NO_X proxy-based method to infer anthropogenic CO_2 emissions (Feng et al., 2024). The method assumes a CO_2-NO_X co-emission relationship during fossil fuel combustion, so that optimized NO_X emissions can indicate the spatial adjustment of anthropogenic CO_2. For comparability, the same MEIC inventory and study period were used. Firstly, the RAPAS system assimilated hourly surface NO_2 observations from China's national air quality monitoring stations to constrain MEIC NO_X and produce posterior estimates. Cell-wise CO_2-to-NO_X emission ratios from the MEIC were then applied to the posterior NO_X to infer anthropogenic CO_2 emissions. Finally, the resulting CO_2 was compared with the posterior from direct XCO_2 assimilation on a uniform 27-km grid, serving as an auxiliary reference for evaluating the robustness and uncertainty of the key-region emission adjustments.

2.5 OSSE experiment

To evaluate the reliability and constraint capability of RegGCAS, this study designed an OSSE experiment. The overall experimental procedure was generally consistent with the emission inversion constrained by real satellite observations, except that the observations and prior emissions were idealized. Specifically, the MEIC emission inventory was first used as the true emissions to drive the WRF-CMAQ model for forward simulations. Then, based on the spatiotemporal sampling characteristics of OCO-2/3, CO_2 concentrations at the corresponding locations were extracted from the simulation results to construct pseudo-observations. Subsequently, the MEIC emissions were uniformly scaled down by 30% to serve as the prior, and the inversion was conducted under the same assimilation configuration as the real inversion (Liu et al., 2017). Finally, by comparing the posterior emissions with the true emissions, we evaluated the capability of RegGCAS to invert anthropogenic CO_2 emissions under idealized observational conditions.

https://doi.org/10.5194/egusphere-2026-3241
Preprint. Discussion started: 13 July 2026

3. Results and discussion

3.1 Anthropogenic CO_2 emissions

Fig. 1(a-c) presents the spatial distribution of anthropogenic CO_2 emissions over mainland China during winter before and after assimilation, as well as their deviations from the MEIC prior. Overall, high-emission areas were primarily distributed in densely populated and economically active regions in eastern coastal and central-eastern China, including Beijing-Tianjin-Hebei (BTH), YRD, the Pearl River Delta, and the Sichuan Basin. Conversely, emissions were relatively low in the northwestern, southwestern, and northeastern regions. Compared with the MEIC, the posterior emissions exhibited an overall upward adjustment at the national scale. The total posterior anthropogenic CO_2 emissions during winter amounted to 2808.3 ± 157.0 Tg, 16.1% higher than the MEIC, indicating a certain underestimation in the MEIC inventory.

The adjustments of posterior CO_2 emissions exhibited distinct spatial heterogeneity, with emission increases mainly located in northern China, particularly in the North China Plain. This may be related to the underestimation of winter heating emissions in the prior inventory. Winter heating in northern China relies heavily on fossil fuels such as coal, and residential coal combustion, along with decentralized heating, contributes substantially to regional emissions (Zhang et al., 2021). However, these emission sources are relatively dispersed, leading to considerable uncertainties in activity level statistics, and a portion of these emissions may not be fully incorporated into the inventory (Li et al., 2017a). Previous studies have indicated that rural residential coal consumption in the North China Plain may be underreported in official statistics, resulting in an underestimation of winter coal combustion emissions in existing inventories (Peng et al., 2019). This justifies the overall upward adjustment of emissions in this region after assimilation.

https://doi.org/10.5194/egusphere-2026-3241
Preprint. Discussion started: 13 July 2026

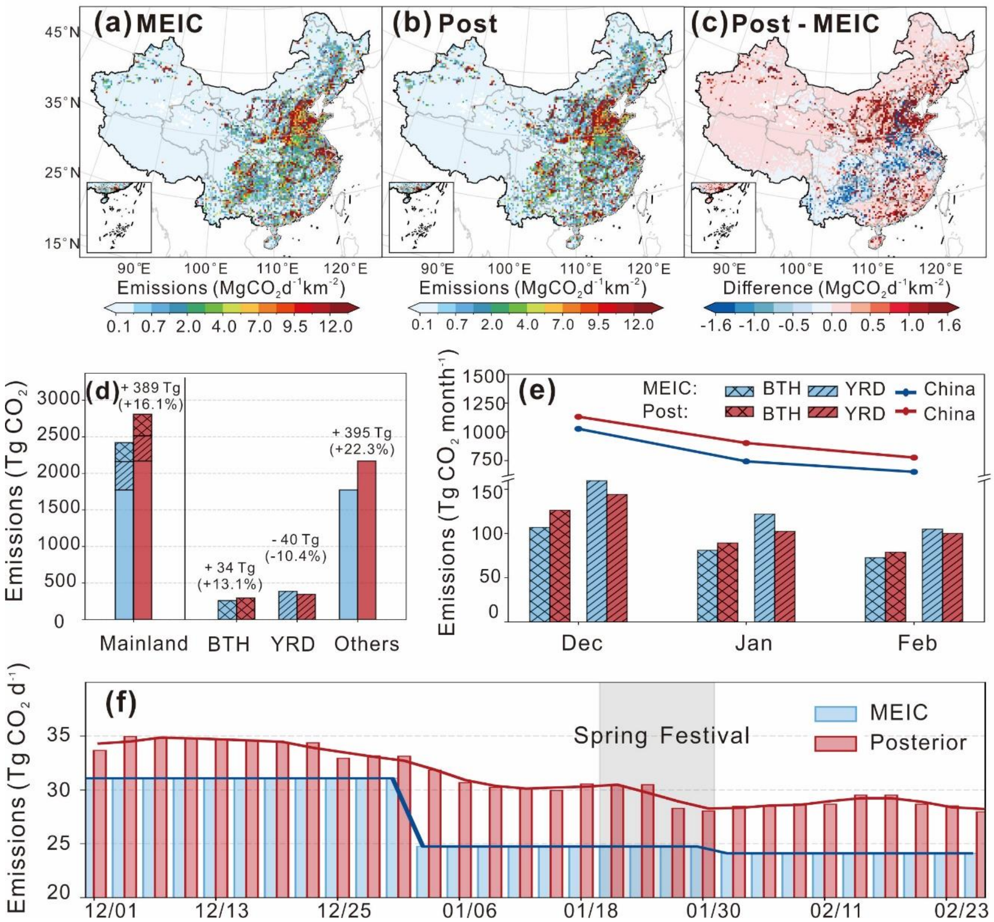

Fig. 1. Anthropogenic CO_2 emissions over mainland China before and after assimilation. (a) MEIC inventory ($MgCO_2$ d^{-1} km^{-2}); (b) posterior emissions ($MgCO_2$ d^{-1} km^{-2}); (c) posterior-minus-prior differences ($MgCO_2$ d^{-1} km^{-2}); (d) winter totals over mainland China, BTH, and YRD ($TgCO_2$); (e) monthly totals ($TgCO_2$ $month^{-1}$); (f) winter daily means ($TgCO_2$ d^{-1}), with gray shading for the Spring Festival.

As two major hotspots for anthropogenic emissions, the BTH and YRD regions accounted for 10.8% and 16.0% of the national total, respectively. For the BTH region, most emissions were mainly distributed in the densely populated urban and industrial areas in the east and south. The total posterior emissions were 294.2 ± 28.9 Tg, 13.1% higher than the MEIC prior, with adjustments primarily occurring in high-emission areas (Fig. 2b-c). For the YRD region, significant downward adjustments of posterior emissions were primarily located in the eastern coastal belt and the major urban clusters (Fig. 2e-f). The total posterior emissions for the YRD were 345.9 ± 46.3 Tg, 10.4% lower than the MEIC,

https://doi.org/10.5194/egusphere-2026-3241
Preprint. Discussion started: 13 July 2026

suggesting a potential overestimated in the MEIC for this region. This discrepancy likely arose from overestimated emission factors. As noted by Feng et al. (2024), economically developed areas such as the YRD generally possessed technological levels and energy utilization efficiencies that surpassed the national average, resulting in relatively lower carbon emission intensities per unit of economic output. Consequently, applying uniform emission factors in the inventory failed to accurately reflect actual emission levels, thereby leading to positively biased prior emissions. In both regions, emissions in most key city centers were adjusted downward, while emissions in suburban and surrounding areas increased. This spatial adjustment pattern likely reflected biases in the spatial disaggregation of the emission inventory. Gridded inventories like MEIC typically rely on proxy variables (e.g., population density and road networks) for spatial downscaling (Zheng et al., 2021). However, these proxy variables are overwhelmingly concentrated in urban centers and struggle to accurately represent high-emission point sources (e.g., factories and power plants) located in urban peripheries or suburban industrial belts. Thus, these inventories tend to allocate excessive emissions to central urban areas, thereby underestimating actual emissions in the peripheries. It is worth noting that, although satellite XCO_2 observations are less sensitive to local emission changes than ground-based observations (Parker et al., 2023), this study, constrained solely by OCO-2/3 XCO_2 observations, still identified a distinct emission adjustment pattern between city centers and their peripheries in high-emission regions. This demonstrates that RegGCAS can not only constrain total regional emissions but also to some extent reflect spatial allocation biases within the urban clusters of these key emission regions.

This study also presents the results derived from the proxy-based method. For the BTH, emission adjustments identified were primarily located in key cities and their surroundings, with downward adjustments in most key city centers. This finding was generally consistent with the direct assimilation results of XCO_2 observations (Fig. 2d). However, the overall CO_2 emissions derived from this method were lower and exhibited a broader extent of downward adjustments, which may be related to the CO_2-to-NO_X ratios used in the conversion. Due to the time lag in updating "bottom-up" inventories, this study adopted the ratios from the 2019 inventory. Previous studies have demonstrated a continuous increase in the CO_2-to-NO_X ratios over East Asia in recent years (Li et al., 2024; Li et al., 2023), and this trend may be even more pronounced in the BTH region, where winter pollution control requirements were more stringent (Xu et al., 2023; Liu et al., 2020). Therefore, continuing to rely on these relatively outdated CO_2-to-NO_X ratios likely led to

https://doi.org/10.5194/egusphere-2026-3241
Preprint. Discussion started: 13 July 2026

an underestimation of actual CO_2 emissions. For the YRD, our results were similar to those from the proxy-based approach, with emission adjustments predominantly downward and concentrated mainly in key urban clusters in the east, particularly in southern Jiangsu Province (Fig. 2g). Overall, the two methods showed relatively consistent emission adjustment patterns in the key regions, which to some extent supports the reliability of the results in this study.

In terms of monthly variations, anthropogenic CO_2 emissions over mainland China, as well as in the BTH and YRD regions, exhibited a continuous monthly declining trend (Fig. 1e). The national posterior emissions remained consistently higher than the prior, with monthly increases of 12.5%, 20.6%, and 17.2% during the winter, indicating that assimilation exerted a more pronounced upward effect on emissions. For the BTH, posterior emissions were higher than the prior, with the most significant upward adjustment (18.4%) in December. For the YRD, posterior emissions were consistently lower than the prior, recording the most substantial decrease (16.0%) in January. In the 3-day assimilation window (Fig. 1f), posterior emissions dropped markedly during the Spring Festival holiday, with a reduction of approximately 2-3 Tg CO_2 d^{-1}, and gradually rebounded thereafter. This indicates that, compared to the prior emissions that only reflect monthly variations, the posterior results better capture the short-term emission fluctuations associated with reduced anthropogenic activities during the Spring Festival and the subsequent post-holiday recovery.

https://doi.org/10.5194/egusphere-2026-3241
Preprint. Discussion started: 13 July 2026

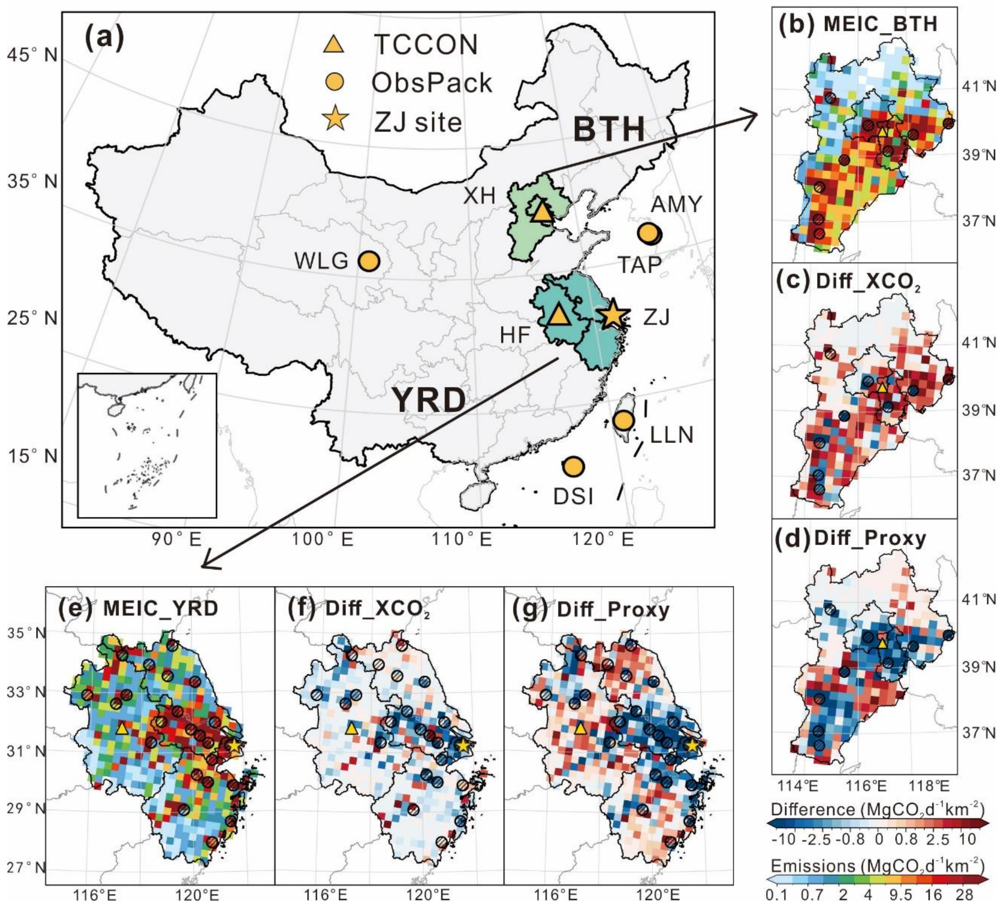

Fig. 2. Spatial distribution of emissions and adjustments ($MgCO_2\ d^{-1}\ km^{-2}$) in the BTH and YRD regions. (a) BTH and YRD locations. Yellow circles denote ObsPack sites; (b-d) BTH: posterior emissions, and emissions adjustments derived from direct XCO_2 assimilation (Diff_XCO_2) and the proxy-based method (Diff_Proxy), respectively; (e-g) same as (b-d) but for YRD. The yellow triangle denotes the XH site (b-d) and HF site (e-g). The yellow five-pointed star denotes the ZJ site. Hatched circles denote key city centers.

3.2 Emission evaluation

We first utilized an OSSE to evaluate the reliability and constraint capability of the RegGCAS. The results revealed that assimilation can effectively utilize pseudo-observations, bringing the emission estimates closer to the MEIC. In terms of regional totals, the national prior emissions were underestimated by 30%, which decreased to 9.6% after assimilation, representing a 68.0% reduction in prior bias. Notably, in the densely

https://doi.org/10.5194/egusphere-2026-3241
Preprint. Discussion started: 13 July 2026

observed BTH region, the total posterior emissions were nearly identical to the true emissions, with a 98.7% reduction in prior bias. In the YRD region, the prior bias was also reduced by 58.0% after assimilation. In terms of spatial distribution (Fig. 3b), the range of negative biases was significantly reduced after assimilation, with emission biases approaching zero in many regions. Meanwhile, certain residual negative biases persisted locally, suggesting that under the current OCO observational coverage, the constraints in some regions may still be insufficient, preventing full recovery of true emissions across all grids. This also implied that the posterior emissions depicted in Fig. 1(b) were still underestimated. However, in some regions (e.g., Guizhou, Hubei, and Hunan), adjustments still deviated from the true emissions (Fig. 3c), primarily due to inadequate local observation coverage (Fig. 3d). Observations in these regions are relatively sparse. Once emissions were over-adjusted in an individual assimilation window, and subsequent observations were insufficient to correct the adjustment, the bias persisted in the following windows.

https://doi.org/10.5194/egusphere-2026-3241
Preprint. Discussion started: 13 July 2026

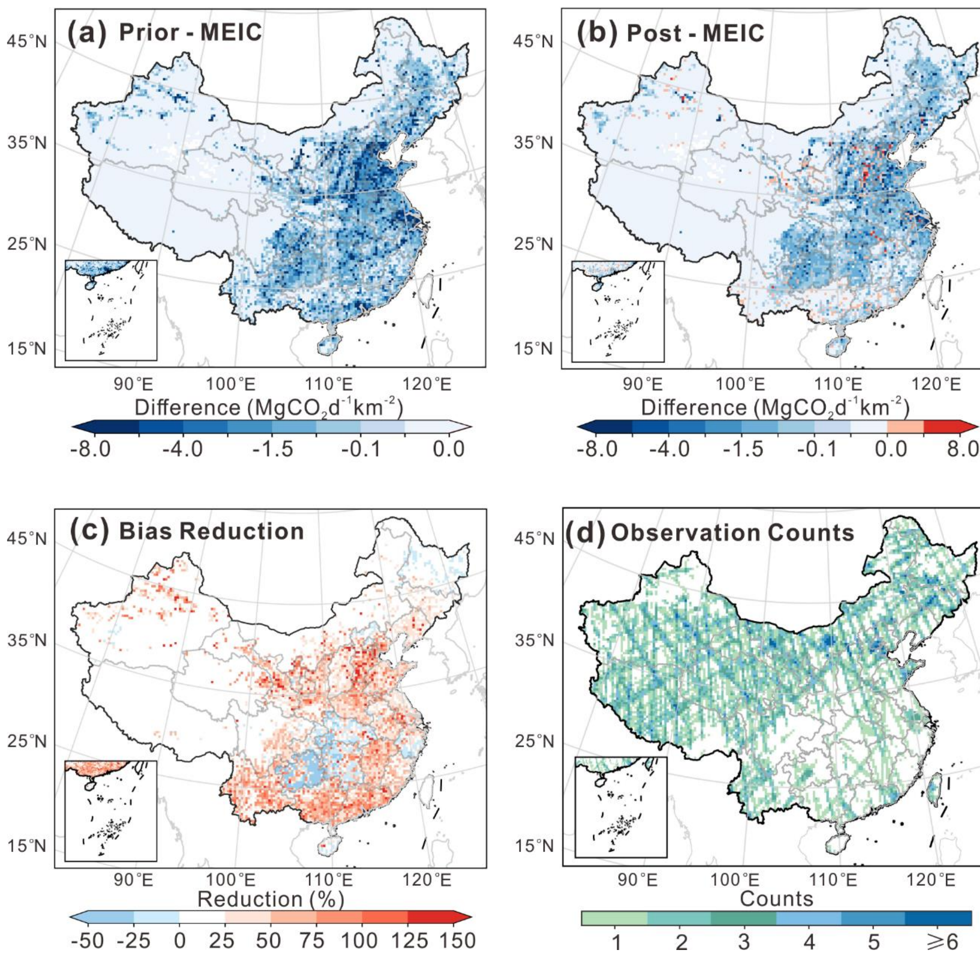

Fig. 3. OSSE results. (a) prior-minus-MEIC differences ($MgCO_2\ d^{-1}\ km^{-2}$); (b) posterior-minus-MEIC differences ($MgCO_2\ d^{-1}\ km^{-2}$); (c) prior bias reduction (%). Reduction = (Posterior - Prior) / (MEIC - Prior) × 100; (d) OCO observation counts.

The results of the assimilated observation consistency analysis (Fig. 4a-c) indicate that, at the national scale, the prior simulated XCO_2 broadly exhibited negative biases, particularly in the North and Northwest China. The adjustments in posterior simulations relative to the prior simulations were generally consistent with the posterior emission adjustments, and were mainly distributed in northern China, where anthropogenic sources were intensive and observations were relatively dense. After assimilation, the posterior simulation biases were significantly reduced. For example, the posterior simulated concentrations in North and Northwest China were increased, significantly improving the

https://doi.org/10.5194/egusphere-2026-3241
Preprint. Discussion started: 13 July 2026

underestimation in the prior simulations. Similarly, posterior simulations effectively alleviated the overestimation in Heilongjiang Province in Northeast China by decreasing concentrations. Statistical results show that after assimilation, the national BIAS was reduced from -0.6 ppm to -0.4 ppm, while the MAE and RMSE decreased by 6.8% and 5.8%, respectively, indicating an improved consistency between the simulations and observations. For key emission regions, the BTH showed notable improvement, with BIAS decreasing from approximately -0.7 ppm to -0.3 ppm, a reduction of 56.5%, and MAE and RMSE were reduced by 14.4% and 12.5%, respectively. In contrast, the YRD region exhibited relatively small changes in statistical metrics, which is largely attributed to the relatively insufficient satellite observational coverage in this region. Nevertheless, the posterior simulation MAE was still reduced by 3.2%.

The evaluation results at the TCCON sites show that the posterior simulations were consistently improved compared to the prior simulations (Fig. 4h-i). Specifically, at the XH site, BIAS was reduced by 28.8%, MAE and RMSE decreased by 14.3% and 15.6%, respectively, and the CORR increased from 0.76 to 0.80. At the HF site, BIAS decreased from -0.6 ppm to -0.3 ppm, a reduction of approximately 50.0%, MAE and RMSE reduced by 14.0% and 14.9%, respectively, and the CORR increased from 0.31 to 0.41. Overall, with a 15.3% average RMSE reduction at both stations, posterior simulations outperformed prior simulations after assimilation.

https://doi.org/10.5194/egusphere-2026-3241
Preprint. Discussion started: 13 July 2026

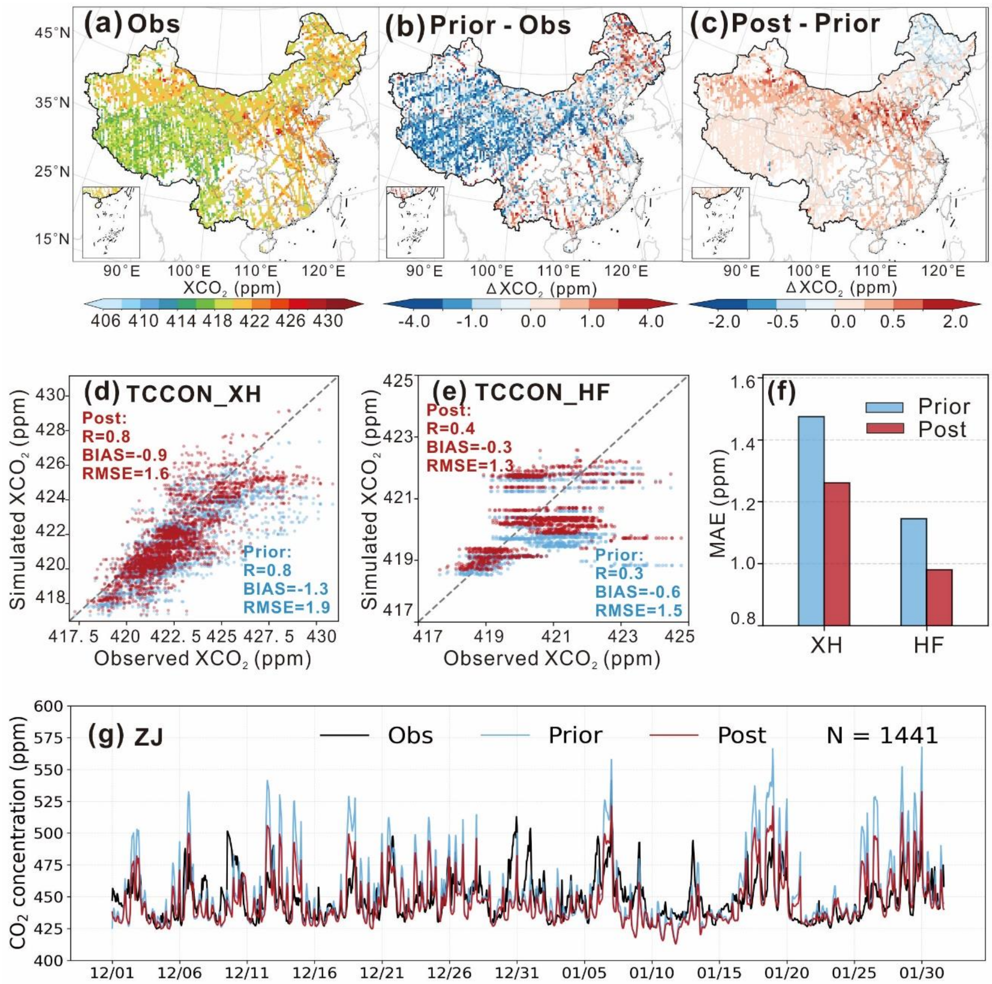

Fig. 4. Evaluation of XCO_2 simulation based on satellite observations and independent site data (ppm). (a-c) OCO-2/3 XCO_2 observations, prior-minus-observation differences, and posterior-minus-observation differences; (d-e) Comparison of simulated and observed XCO_2 at the XH and HF sites; (f) MAE of prior and posterior simulations at two sites; (g) Time series of observed near-surface CO_2 concentrations and prior and posterior simulations at the Shanghai ZJ site.

Table 1 presents the independent validation results at the ObsPack ground-based sites. At the TAP site, MAE decreased from 2.1 ppm to 1.8 ppm, RMSE dropped by 17.4%, and the CORR increased from 0.89 to 0.94. The DSI, LLN, and WLG sites also exhibited certain improvements, with their posterior MAE and RMSE decreasing by approximately 2.5%-9.0% and 3.3%-5.0%, respectively. Although posterior MAE at the AMY site was slightly higher than the prior result, its RMSE still decreased by 8.9%. The varying degrees

https://doi.org/10.5194/egusphere-2026-3241
Preprint. Discussion started: 13 July 2026

of improvement among sites are mainly due to differences in site environments and their sensitivity to anthropogenic emission changes. TAP, DSI, and AMY are all located in coastal or offshore environments, where observed concentrations are highly susceptible to the combined effects of regional transport and local meteorological processes (Lin et al., 2018). WLG and LLN are high-altitude background stations with relatively weak influences from surrounding local anthropogenic sources, making them more sensitive to large-scale background variations and long-range transport. Consequently, in addition to the emissions, their simulation errors are closely related to lateral boundary inputs, background field, and transport errors (Guo et al., 2020; Ou-Yang et al., 2025). Overall, most sites showed improvement after assimilation, with BIAS decreasing by 8.7% and RMSE by 7.7%, indicating that the assimilation of OCO XCO_2 observations can effectively improve the estimation of anthropogenic CO_2 emissions and enhance the capability to simulate CO_2 concentrations.

Table 1. Validation statistics for the prior and posterior simulated CO_2 concentrations at the ObsPack ground-based sites and the ZJ site.

Site	**Prior**				**Posterior**			
	BIAS (ppm)	**MAE (ppm)**	**RMSE (ppm)**	**CORR**	**BIAS (ppm)**	**MAE (ppm)**	**RMSE (ppm)**	**CORR**
TAP	-0.35	2.11	2.65	0.89	-0.32	1.77	2.19	0.94
DSI	-1.53	2.10	2.79	0.65	-1.27	1.91	2.65	0.66
LLN	-0.06	1.19	1.51	0.47	0.14	1.16	1.46	0.53
WLG	-1.01	1.21	1.63	0.70	-0.79	1.13	1.57	0.68
AMY	0.94	1.90	2.47	0.74	1.03	1.94	2.25	0.75
ZJ	4.34	15.23	21.95	0.56	-2.38	11.90	16.42	0.58

In addition, the near-surface CO_2 comparison at the Shanghai ZJ urban site provides an independent evaluation of the posterior emissions under strong urban influence. The prior simulation exhibits a positive bias relative to observations, especially during high CO_2 episodes (Fig. 4g), which is consistent with the overestimated prior emissions in this region. Following optimization, the posterior simulation effectively mitigates this

https://doi.org/10.5194/egusphere-2026-3241
Preprint. Discussion started: 13 July 2026

overestimation. Although the posterior simulation retains a residual negative bias, primarily attributable to the spatial representation error between grid-mean model concentrations and point-scale urban measurements heavily impacted by intense local emissions (Tolk et al., 2008), the MAE and RMSE decrease by 21.9% and 25.2%, respectively, while the CORR slightly increases from 0.56 to 0.58. This marked reduction in overestimation provides compelling evidence that the system can robustly constrain emissions even in urban regions characterized by dense anthropogenic sources.

3.3 System sensitivity analysis

To evaluate the sensitivity of the inversion results to different system configurations, this study conducted a series of sensitivity experiments focusing on factors including the background fields, observation settings, prior anthropogenic emission, biogenic carbon fluxes, localization scales, as well as background and observation errors (Table 2). Among these, the localization scale primarily influences the spatial range of observational information (Hunt et al., 2007), and the background and observation errors affect the assimilation results by altering the relative weights between the prior and observations (Evensen, 2003). The results demonstrated that the posterior total deviations relative to the BASE were consistently constrained within ± 3.5% for a subset of sensitivity experiments, including those on different localization scales (LOC_300, LOC_800), background error levels (ERR_BKG0.2, ERR_BKG0.8), and observation error magnitudes (ERR_OBS0.5, ERR_OBS2). This demonstrated that the two-step inversion strategy can effectively mitigate the sensitivity of the inversion results to system parameters, indicating the robustness of the system.

When assimilating only OCO-2 (OBS_OCO2) or only OCO-3 (OBS_OCO3), the posterior totals decreased by 1.1% and 10.4% relative to BASE, respectively. Based on the OSSE results, the BASE experiment still underestimated emissions under current observations, while both single-satellite assimilation experiments yielded even lower emission results than BASE. This indicates that a single satellite has inherent deficiencies in spatial coverage and sampling uniformity, making it insufficient to fully constrain regional emissions and necessitating the joint assimilation of multiple observational datasets.

https://doi.org/10.5194/egusphere-2026-3241
Preprint. Discussion started: 13 July 2026

Table 2. Configurations of the sensitivity experiments and their posterior emission differences relative to the BASE experiment.

Name	BKG	Anth	Bio	Obs	Loc (km)	BKG_ Error (%)	OBS_ Error (factor)	Diff (%)
BASE	GCAS	MEIC	BEPS	O2+O3	500	40	1.0	0.0
BKG_CT	Carbon Tracker	MEIC	BEPS	O2+O3	500	40	1.0	-10.3
OBS_OCO2	GCAS	MEIC	BEPS	O2	500	40	1.0	-1.1
OBS_OCO3	GCAS	MEIC	BEPS	O3	500	40	1.0	-10.4
BIO_CASA	GCAS	MEIC	CASA	O2+O3	500	40	1.0	-11.7
EDGAR_PRI	GCAS	EDGAR	BEPS	O2+O3	500	40	1.0	+5.7
LOC_300	GCAS	MEIC	BEPS	O2+O3	300	40	1.0	-0.3
LOC_800	GCAS	MEIC	BEPS	O2+O3	800	40	1.0	-1.5
ERR_BKG0.2	GCAS	MEIC	BEPS	O2+O3	500	20	1.0	-1.4
ERR_BKG0.8	GCAS	MEIC	BEPS	O2+O3	500	80	1.0	+1.7
ERR_OBS0.5	GCAS	MEIC	BEPS	O2+O3	500	40	0.5	-1.5
ERR_OBS2	GCAS	MEIC	BEPS	O2+O3	500	40	2.0	+3.3

Note: BKG denotes inversion background field; Anth represents prior anthropogenic CO_2 emissions; Bio denotes biogenic CO_2 fluxes; Obs denotes assimilated OCO satellite observations. O2 and O3 refer to OCO-2 and OCO-3 data, and O2+O3 represents their joint assimilation. Loc is the assimilation localization scale. BKG_Error represents background error. OBS_Error denotes the prescribed observation error scaling factor. Diff indicates the relative difference in posterior anthropogenic emissions between sensitivity tests and the BASE case.

Due to the long atmospheric lifetime of CO_2, background concentrations contribute substantially to the total CO_2 concentrations (Mustafa et al., 2021). Consequently, when biases exist in the background fields, the inversion system tends to compensate for them by adjusting anthropogenic emissions (Pisso et al., 2019). When using the Carbon Tracker background field (BKG_CT), the total posterior emissions decreased by 10.3% relative to BASE, indicating that discrepancies in background concentrations exert a relatively substantial impact on the emission inversion. In the biogenic carbon flux perturbation experiment (BIO_CASA), posterior anthropogenic emissions decreased by 11.7% compared to the BASE. Compared to BEPS, the Carnegie-Ames-Stanford Approach (CASA) product exhibited stronger positive fluxes at the national scale, particularly in the central-eastern, North China, and Northeast China regions, thereby elevating the natural background CO_2 levels. To match satellite XCO_2 observations, the assimilation system offsets this higher biogenic background by producing correspondingly lower posterior anthropogenic emissions.

https://doi.org/10.5194/egusphere-2026-3241
Preprint. Discussion started: 13 July 2026

When employing EDGAR as the prior inventory (EDGAR_PRI), posterior anthropogenic emissions increased by 5.7% relative to BASE. Although the emissions in the EDGAR inventory were higher than those in the MEIC, prior inventory differences had a limited impact on inversion results. For instance, the prior difference between EDGAR and MEIC increased from 16.2 Tg in the first window to 37.8 Tg in the last window, whereas the corresponding posterior difference narrowed from 11.1 Tg to 2.1 Tg. This indicated that observational constraints effectively mitigated the influence of prior inventory differences on the posterior results.

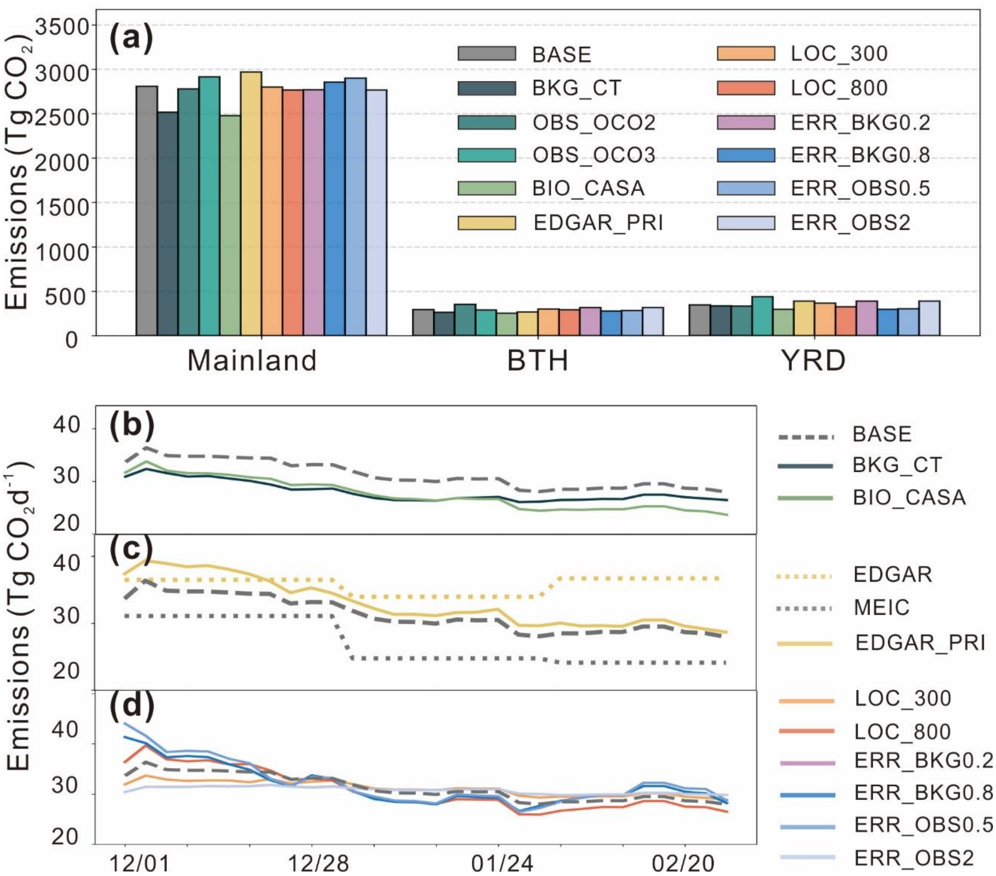

Fig. 5. Sensitivity experiment results. (a) total anthropogenic CO_2 emissions over mainland China and key regions under different sensitivity experiments ($TgCO_2$); (b-d) temporal variations of national anthropogenic CO_2 emissions under different system configurations ($TgCO_2\ d^{-1}$).

Comparing the inversion results across sensitivity experiments over time (Fig. 5b-d), it can be observed that in the first assimilation window, the regional emission estimates

https://doi.org/10.5194/egusphere-2026-3241
Preprint. Discussion started: 13 July 2026

varied across experiments, with a standard deviation of 4.4 Tg and a range of 13.6 Tg. As assimilation advanced, the dispersion gradually decreased. By the final window, the standard deviation and range had been reduced by 52.3% and 39.7%, respectively. This indicated that although different system assumptions introduce certain discrepancies during the initial phase of assimilation, the inversion results gradually converged as more observations were assimilated, ultimately achieving good consistency. Based on all sensitivity experiments, the uncertainty of regional total emission estimates was 5.6%, thus verifying the high reliability of the posterior emission estimates.

4. Summary and conclusions

Accurately quantifying anthropogenic CO_2 emissions is essential for evaluating carbon budgets and formulating effective mitigation strategies. However, structural uncertainties and spatial allocation biases in traditional "bottom-up" inventories significantly hinder our understanding of anthropogenic carbon forcing. To independently evaluate and optimize these inventories, this study extended RegGCAS, a regional carbon assimilation system based on the WRF-CMAQ atmospheric transport model and the EnKF algorithm. By jointly assimilating OCO-2 and OCO-3 XCO_2 observations, we inverted anthropogenic CO_2 emissions over mainland China during the winter of 2022-2023.

Our results yielded national total posterior emissions of 2808.3 ± 157.0 Tg, which is 16.1% higher than the MEIC inventory, indicating a systematic underestimation in winter prior emissions. These emission adjustments exhibited significant regional heterogeneity. Specifically, emissions in the BTH region were revised upward by 13.1%, largely due to the underestimation of winter heating emissions. Conversely, emissions in the YRD were adjusted downward by 10.4%, reflecting positively biased emission factors in MEIC. Spatially, the posterior estimates corrected local emission intensities, effectively resolving the emission gradients between urban centers and surrounding suburban areas. Temporally, the assimilated results captured pronounced seasonal and short-term variations, most notably the emission decline during the Spring Festival, demonstrating the system's enhanced capability to respond to short-term anthropogenic activity fluctuations. System reliability was validated through an OSSE, which showed that assimilation reduced prior emission biases by approximately 68%. Furthermore, independent validations demonstrated that the posterior simulations reduced the RMSEs against assimilated OCO-2/3 XCO_2, TCCON XCO_2, ObsPack surface CO_2, and dedicated high-precision urban site

https://doi.org/10.5194/egusphere-2026-3241
Preprint. Discussion started: 13 July 2026

observations by 5.8%, 15.3%, 7.7%, and 25.2%, respectively, confirming the enhanced accuracy of the posterior estimates and simulated concentrations.

Compared to previous studies that primarily focused on specific point sources or relied on sparsely distributed ground-based observations in limited urban areas, this study advances the field by utilizing satellite XCO_2 constraints to achieve a targeted inversion of anthropogenic emissions at a national scale. Our findings align with and expand upon existing knowledge. The upward adjustment in the BTH region corroborates evidence of underreported coal consumption, while the downward adjustment in the YRD reflects higher regional energy efficiencies that uniform emission factors fail to capture. Moreover, the distinct urban-suburban correction pattern highlights the limitations of proxy-based downscaling in current gridded inventories, which frequently allocate excessive emissions to urban cores while underestimating major industrial sources in suburban belts. Our results are also consistent with previous proxy-based inversion studies relying on co-emitted NO_X; however, direct XCO_2 assimilation overcomes the inherent uncertainties associated with the lagged updates of prior CO_2-to-NO_X ratios.

Despite the robustness of this assimilation framework, certain limitations must be acknowledged. As indicated by the OSSE results, existing OCO footprints provide inadequate observation coverage over certain regions (e.g., Guizhou), leading to residual local emission biases. Furthermore, sensitivity analyses revealed that while the inversion is resilient to most internal parameter settings, it exhibits moderate sensitivity to biogenic carbon fluxes and background CO_2 concentrations. Because of the long atmospheric lifetime of CO_2, discrepancies in background fields can inadvertently force the assimilation system into excessive anthropogenic emission adjustments. Finally, although this study intentionally focused on the winter season, the inherent structural biases identified within the bottom-up inventories are likely applicable throughout the year. Future efforts should prioritize the joint assimilation of multi-source surface and satellite observations, along with carbon isotope measurements, to better decouple natural and anthropogenic emissions, thereby extending reliable top-down emission constraints to an annual scale.

Ultimately, this study demonstrates that satellite XCO_2 assimilation provides an effective top-down constraint to correct anthropogenic CO_2 emission biases, enhancing the capability of models to capture short-term temporal fluctuations and fine-scale spatial gradients. Crucially, the identification of these systematic regional disparities provides valuable guidance for refining the compilation and proxy-based downscaling methods of future bottom-up emission inventories. Furthermore, the implementation of RegGCAS provides a reliable, operational regional inversion framework. Such an independent and verifiable top-down carbon monitoring system is essential for informing robust, science-based climate mitigation policies.

Code availability

The code of the RegGCAS system is available to the community and can be accessed upon request from Shuzhuang Feng (fengsz@nju.edu.cn) at Nanjing University.

Data availability

The inversion results of this study are available online (https://doi.org/10.5281/zenodo.20605680)

Author contributions

SQ and SF designed the research. SQ and HZ processed the data. SQ performed model simulations, analyzed the results, and wrote the manuscript. FJ, CW, YS, MJ, HW, YZ, and WJ discussed and revised the manuscript.

Competing interest

The author declares no conflicts of interest relevant to this study.

Acknowledgments

This work is supported by the National Key Research and Development Program of China (Grant Nos. 2023YFB3907404 and 2022YFB3904801), the National Natural Science Foundation of China (Grant No. 42305116), and the Natural Science Foundation of Jiangsu Province of China (Grant No. BK20230801). We also gratefully acknowledge the High-Performance Computing Center (HPCC) of Nanjing University for supporting the numerical calculations in this paper on its blade cluster system.

References

Bocquet, M., Elbern, H., Eskes, H., Hirtl, M., Žabkar, R., Carmichael, G. R., Flemming, J., Inness, A., Pagowski, M., Pérez Camaño, J. L., Saide, P. E., San Jose, R., Sofiev, M., Vira, J., Baklanov, A., Carnevale, C., Grell, G., and Seigneur, C.: Data assimilation in atmospheric chemistry models: current status and future prospects for coupled chemistry meteorology models, Atmospheric Chemistry and Physics, 15, 5325-5358, https://doi.org/10.5194/acp-15-5325-2015, 2015.

Byun, D. and Schere, K. L.: Review of the Governing Equations, Computational Algorithms, and Other Components of the Models-3 Community Multiscale Air Quality (CMAQ) Modeling System, Applied Mechanics Reviews, 59, 51-57, https://doi.org/10.1115/1.2128636, 2006.

Chevallier, F. and Broquet, G.: Atmospheric inversions for carbon dioxide and methane at a national scale, Natl Sci Rev, 12, nwaf063, https://doi.org/10.1093/nsr/nwaf063, 2025.

Eldering, A., Taylor, T. E., O'Dell, C. W., and Pavlick, R.: The OCO-3 mission: measurement objectives and expected performance based on 1 year of simulated data, Atmos. Meas. Tech., 12, 2341-2370, 10.5194/amt-12-2341-2019, 2019.

Evensen, G.: The Ensemble Kalman Filter: theoretical formulation and practical implementation, Ocean Dynamics, 53, 343-367, https://doi.org/10.1007/s10236-003-0036-9, 2003.

Feng, S., Jiang, F., Zhang, Y., Chen, H., Zhuang, H., Wang, S., Bai, S., Wang, H., and Ju, W.: High-resolution regional inversion reveals overestimation of anthropogenic methane emissions in China, Atmospheric Chemistry and Physics, 25, 15121-15143, https://doi.org/10.5194/acp-25-15121-2025, 2025.

Feng, S., Jiang, F., Wang, H., Liu, Y., He, W., Wang, H., Shen, Y., Zhang, L., Jia, M., Ju, W., and Chen, J. M.: China's fossil fuel CO2 emissions estimated using surface observations of coemitted NO2, Environ Sci Technol, 58, 8299-8312, https://doi.org/10.1021/acs.est.3c07756, 2024.

Feng, S., Jiang, F., Wu, Z., Wang, H., He, W., Shen, Y., Zhang, L., Zheng, Y., Lou, C., Jiang, Z., and Ju, W.: A Regional multi-Air Pollutant Assimilation System (RAPAS v1.0) for emission estimates: system development and application, Geoscientific Model Development, 16, 5949-5977, https://doi.org/10.5194/gmd-16-5949-2023, 2023.

Flowerdew, J.: Towards a theory of optimal localisation, Tellus A: Dynamic Meteorology and Oceanography, 67, 25257, https://doi.org/10.3402/tellusa.v67.25257, 2015.

Friedlingstein, P., O'Sullivan, M., Jones, M. W., Andrew, R. M., Hauck, J., Landschützer, P., Le Quéré, C., Li, H., Luijkx, I. T., Olsen, A., Peters, G. P., Peters, W., Pongratz, J., Schwingshackl, C., Sitch, S., Canadell, J. G., Ciais, P., Jackson, R. B., Alin, S. R., Arneth, A., Arora, V., Bates, N. R., Becker, M., Bellouin, N., Berghoff, C. F., Bittig, H. C., Bopp, L., Cadule, P., Campbell, K., Chamberlain, M. A., Chandra, N., Chevallier, F., Chini, L. P., Colligan, T., Decayeux, J., Djeutchouang, L. M., Dou, X., Duran Rojas, C., Enyo, K., Evans, W., Fay, A. R., Feely, R. A., Ford, D. J., Foster, A., Gasser, T., Gehlen, M., Gkritzalis, T., Grassi, G., Gregor, L., Gruber, N., Gürses, Ö., Harris, I., Hefner, M., Heinke, J., Hurtt, G. C., Iida, Y., Ilyina, T., Jacobson, A. R., Jain, A. K., Jarníková, T., Jersild, A., Jiang, F., Jin, Z., Kato, E., Keeling, R. F., Klein Goldewijk, K., Knauer, J., Korsbakken, J. I., Lan, X., Lauvset, S. K., Lefèvre, N., Liu, Z., Liu, J., Ma, L., Maksyutov, S., Marland, G., Mayot, N., McGuire, P. C., Metzl, N., Monacci, N. M., Morgan, E. J., Nakaoka, S.-I., Neill, C., Niwa, Y., Nützel, T., Olivier, L., Ono, T., Palmer, P. I., Pierrot, D., Qin, Z., Resplandy, L., Roobaert, A., Rosan, T. M., Rödenbeck, C., Schwinger, J., Smallman, T. L., Smith, S. M., Sospedra-Alfonso, R., Steinhoff, T., Sun, Q., Sutton, A. J., Séférian, R., Takao, S., Tatebe, H., Tian, H., Tilbrook, B., Torres, O., Tourigny, E., Tsujino, H., Tubiello, F., van der Werf, G., Wanninkhof, R., Wang, X., Yang, D., Yang,

https://doi.org/10.5194/egusphere-2026-3241
Preprint. Discussion started: 13 July 2026

X., Yu, Z., Yuan, W., Yue, X., Zaehle, S., Zeng, N., and Zeng, J.: Global Carbon Budget 2024, Earth System Science Data, 17, 965-1039, https://doi.org/10.5194/essd-17-965-2025, 2024.

Fuentes Andrade, B., Buchwitz, M., Reuter, M., Bovensmann, H., Richter, A., Boesch, H., and Burrows, J. P.: A method for estimating localized CO2 emissions from co-located satellite XCO2 and NO2 images, Atmospheric Measurement Techniques, 17, 1145-1173, https://doi.org/10.5194/amt-17-1145-2024, 2024.

Gaspari, G. and Cohn, S. E.: Construction of correlation functions in two and three dimensions, Quarterly Journal of the Royal Meteorological Society, 125, 723-757, https://doi.org/10.1002/qj.49712555417, 1999.

Guo, M., Fang, S., Liu, S., Liang, M., Wu, H., Yang, L., Li, Z., Liu, P., and Zhang, F.: Comparison of atmospheric CO2, CH4, and CO at two stations in the Tibetan Plateau of China, Earth and Space Science, 7, e2019EA001051, https://doi.org/10.1029/2019ea001051, 2020.

Guo, W., Shi, Y., Liu, Y., and Su, M.: CO2 emissions retrieval from coal-fired power plants based on OCO-2/3 satellite observations and a Gaussian plume model, Journal of Cleaner Production, 397, 136525, https://doi.org/10.1016/j.jclepro.2023.136525, 2023.

Houtekamer, P. L. and Mitchell, H. L.: A Sequential ensemble Kalman filter for atmospheric data assimilation, Monthly Weather Review, 129, 123-137, https://doi.org/10.1175/1520-0493(2001)129<0123:ASEKFF>2.0.CO;2, 2001.

Hua, Y., Zhao, X., and Sun, W.: Estimation of anthropogenic CO2 emissions at different scales for assessing SDG indicators: Method and application, Journal of Cleaner Production, 414, 137547, https://doi.org/10.1016/j.jclepro.2023.137547, 2023.

Hunt, B. R., Kostelich, E. J., and Szunyogh, I.: Efficient data assimilation for spatiotemporal chaos: a local ensemble transform Kalman filter, Physica D: Nonlinear Phenomena, 230, 112-126, https://doi.org/10.1016/j.physd.2006.11.008, 2007.

IPCC: 2019 Refinement to the 2006 IPCC Guidelines for National Greenhouse Gas Inventories, Intergovernmental Panel on Climate Change, Switzerland, 2019.

Janssens-Maenhout, G., Pinty, B., Dowell, M., Zunker, H., Andersson, E., Balsamo, G., Bézy, J. L., Brunhes, T., Bösch, H., Bojkov, B., Brunner, D., Buchwitz, M., Crisp, D., Ciais, P., Counet, P., Dee, D., Denier van der Gon, H., Dolman, H., Drinkwater, M. R., Dubovik, O., Engelen, R., Fehr, T., Fernandez, V., Heimann, M., Holmlund, K., Houweling, S., Husband, R., Juvyns, O., Kentarchos, A., Landgraf, J., Lang, R., Löscher, A., Marshall, J., Meijer, Y., Nakajima, M., Palmer, P. I., Peylin, P., Rayner, P., Scholze, M., Sierk, B., Tamminen, J., and Veefkind, P.: Toward an operational anthropogenic CO2 emissions monitoring and verification support capacity, Bulletin of the American Meteorological Society, 101, E1439-E1451, https://doi.org/10.1175/bams-d-19-0017.1, 2020.

Jiang, F., Wang, H., Chen, J. M., Ju, W., Tian, X., Feng, S., Li, G., Chen, Z., Zhang, S., Lu, X., Liu, J., Wang, H., Wang, J., He, W., and Wu, M.: Regional CO2 fluxes from 2010 to 2015 inferred from GOSAT XCO2 retrievals using a new version of the Global Carbon Assimilation System, Atmospheric Chemistry and Physics, 21, 1963-1985, https://doi.org/10.5194/acp-21-1963-2021, 2021.

Juchem, H., Maier, F., Levin, I., Jordan, A., Pöhler, D., Rosendahl, C., Della Coletta, J., Preunkert, S., and Hammer, S.: Challenges and benefits of using NOx as a quantitative proxy for fossil fuel CO2 in an urban area based on radiocarbon measurements, Atmospheric Chemistry and Physics, 25, 18373-18388, https://doi.org/10.5194/acp-25-18373-2025, 2025.

Konovalov, I. B., Berezin, E. V., Ciais, P., Broquet, G., Zhuravlev, R. V., and Janssens-Maenhout, G.: Estimation of fossil-fuel CO2 emissions using satellite measurements of "proxy" species, Atmospheric Chemistry and Physics, 16, 13509-13540, https://doi.org/10.5194/acp-16-13509-2016, 2016.

Lei, R., Feng, S., Danjou, A., Broquet, G., Wu, D., Lin, J. C., O'Dell, C. W., and Lauvaux, T.: Fossil fuel CO2 emissions over metropolitan areas from space: A multi-model analysis of OCO-2 data over Lahore, Pakistan, Remote Sensing of Environment, 264, 112625, https://doi.org/10.1016/j.rse.2021.112625, 2021.

Li, H., Qiu, J., and Zheng, B.: Air-pollution-satellite-based CO2 emission inversion: system evaluation, sensitivity analysis, and future research direction, Atmospheric Chemistry and Physics, 25, 1949-1963, https://doi.org/10.5194/acp-25-1949-2025, 2025.

Li, H., Zheng, B., Lei, Y., Hauglustaine, D., Chen, C., Lin, X., Zhang, Y., Zhang, Q., and He, K.: Trends and drivers of anthropogenic NOx emissions in China since 2020, Environ Sci Ecotechnol, 21, 100425, 10.1016/j.ese.2024.100425, 2024.

Li, M., Liu, H., Geng, G., Hong, C., Liu, F., Song, Y., Tong, D., Zheng, B., Cui, H., Man, H., Zhang, Q., and He, K.: Anthropogenic emission inventories in China: a review, National Science Review, 4, 834-866, https://doi.org/10.1093/nsr/nwx150, 2017a.

Li, M., Zhang, Q., Kurokawa, J.-i., Woo, J.-H., He, K., Lu, Z., Ohara, T., Song, Y., Streets, D. G., Carmichael, G. R., Cheng, Y., Hong, C., Huo, H., Jiang, X., Kang, S., Liu, F., Su, H., and Zheng, B.: MIX: a mosaic Asian anthropogenic emission inventory under the international collaboration framework of the MICS-Asia and HTAP, Atmospheric Chemistry and Physics, 17, 935-963, https://doi.org/10.5194/acp-17-935-2017, 2017b.

Li, S., Wang, S., Wu, Q., Zhang, Y., Ouyang, D., Zheng, H., Han, L., Qiu, X., Wen, Y., Liu, M., Jiang, Y., Yin, D., Liu, K., Zhao, B., Zhang, S., Wu, Y., and Hao, J.: Emission trends of air pollutants and CO2 in China from 2005 to 2021, Earth System Science Data, 15, 2279-2294, https://doi.org/10.5194/essd-15-2279-2023, 2023.

Lian, J., Lauvaux, T., Utard, H., Bréon, F.-M., Broquet, G., Ramonet, M., Laurent, O., Albarus, I., Chariot, M., Kotthaus, S., Haeffelin, M., Sanchez, O., Perrussel, O., Denier van der Gon, H. A., Dellaert, S. N. C., and Ciais, P.: Can we use atmospheric CO2 measurements to verify emission trends reported by cities? Lessons from a 6-year atmospheric inversion over Paris, Atmospheric Chemistry and Physics, 23, 8823-8835, https://doi.org/10.5194/acp-23-8823-2023, 2023.

Lin, X., Ciais, P., Bousquet, P., Ramonet, M., Yin, Y., Balkanski, Y., Cozic, A., Delmotte, M., Evangeliou, N., Indira, N. K., Locatelli, R., Peng, S., Piao, S., Saunois, M., Swathi, P. S., Wang, R., Yver-Kwok, C., Tiwari, Y. K., and Zhou, L.: Simulating CH4 and CO2 over South and East Asia using the zoomed chemistry transport model LMDz-INCA, Atmospheric Chemistry and Physics, 18, 9475-9497, https://doi.org/10.5194/acp-18-9475-2018, 2018.

Liu, S., Chu, Y., and Hu, J.: Clean air actions and air quality improvements — Beijing-Tianjin-Hebei and surrounding areas, China, 2013-2019, China CDC Weekly, 2, 418-421, 10.46234/ccdcw2020.107, 2020.

Liu, X., Mizzi, A. P., Anderson, J. L., Fung, I. Y., and Cohen, R. C.: Assimilation of satellite NO2 observations at high spatial resolution using OSSEs, Atmospheric Chemistry and Physics, 17, 7067-7081, 10.5194/acp-17-7067-2017, 2017.

Miyazaki, K., Eskes, H., Sudo, K., Boersma, K. F., Bowman, K., and Kanaya, Y.: Decadal changes in global surface NOx emissions from multi-constituent satellite data assimilation, Atmospheric Chemistry and Physics, 17, 807-837, https://doi.org/10.5194/acp-17-807-2017, 2017.

Mustafa, F., Bu, L., Wang, Q., Yao, N., Shahzaman, M., Bilal, M., Aslam, R. W., and Iqbal, R.: Neural-network-based estimation of regional-scale anthropogenic CO2 emissions using an Orbiting Carbon Observatory-2

https://doi.org/10.5194/egusphere-2026-3241
Preprint. Discussion started: 13 July 2026

(OCO-2) dataset over East and West Asia, Atmospheric Measurement Techniques, 14, 7277-7290, https://doi.org/10.5194/amt-14-7277-2021, 2021.

Nassar, R., Mastrogiacomo, J.-P., Bateman-Hemphill, W., McCracken, C., MacDonald, C. G., Hill, T., O'Dell, C. W., Kiel, M., and Crisp, D.: Advances in quantifying power plant CO2 emissions with OCO-2, Remote Sensing of Environment, 264, 112579, https://doi.org/10.1016/j.rse.2021.112579, 2021.

Oney, B., Gruber, N., Henne, S., Leuenberger, M., and Brunner, D.: A CO-based method to determine the regional biospheric signal in atmospheric CO2, Tellus B: Chemical and Physical Meteorology, 69, 1353388, https://doi.org/10.1080/16000889.2017.1353388, 2017.

Ou-Yang, C. F., Wang, J. L., Lin, C. C., Chiu, C. Y., Liu, W. T., Lan, X., Neff, D., Miller, J. B., Michel, S. E., Vaughn, B. H., Chiu, Y. C., Yu, J. Y., Cheng, C. C., Schnell, R. C., White, J. W. C., and Lin, N. H.: Long-term measurements of CO2, CH4, and isotopic ratios of CO2 in the Western Pacific: trends, variations, and implications, Journal of Geophysical Research: Atmospheres, 130, e2024JD042255, https://doi.org/10.1029/2024jd042255, 2025.

Parker, H. A., Laughner, J. L., Toon, G. C., Wunch, D., Roehl, C. M., Iraci, L. T., Podolske, J. R., McKain, K., Baier, B., and Wennberg, P. O.: Inferring the vertical distribution of CO and CO2 from TCCON total column values using the TARDISS algorithm, Atmospheric Measurement Techniques, 16, 2601–2625, https://doi.org/10.5194/amt-16-2601-2023, 2023.

Peng, L., Zhang, Q., Yao, Z., Mauzerall, D. L., Kang, S., Du, Z., Zheng, Y., Xue, T., and He, K.: Underreported coal in statistics: A survey-based solid fuel consumption and emission inventory for the rural residential sector in China, Applied Energy, 235, 1169-1182, https://doi.org/10.1016/j.apenergy.2018.11.043, 2019.

Pisso, I., Patra, P., Takigawa, M., Machida, T., Matsueda, H., and Sawa, Y.: Assessing Lagrangian inverse modelling of urban anthropogenic CO2 fluxes using in situ aircraft and ground-based measurements in the Tokyo area, Carbon Balance Manag, 14, 6, https://doi.org/10.1186/s13021-019-0118-8, 2019.

Randerson, J. T., van der Werf, G. R., Giglio, L., Collatz, G. J., and Kasibhatla, P. S.: Global Fire Emissions Database, Version 4.1 (GFED v4) [dataset], https://doi.org/10.3334/ORNLDAAC/1293, 2017.

Schuh, A. E., Jacobson, A. R., Basu, S., Weir, B., Baker, D., Bowman, K., Chevallier, F., Crowell, S., Davis, K. J., Deng, F., Denning, S., Feng, L., Jones, D., Liu, J., and Palmer, P. I.: Quantifying the impact of atmospheric transport uncertainty on CO2 surface flux estimates, Global Biogeochem Cycles, 33, 484-500, https://doi.org/10.1029/2018GB006086, 2019.

Skamarock, W. C. and Klemp, J. B.: A time-split nonhydrostatic atmospheric model for weather research and forecasting applications, Journal of Computational Physics, 227, 3465-3485, https://doi.org/10.1016/j.jcp.2007.01.037, 2008.

Super, I., Scarpelli, T., Droste, A., and Palmer, P. I.: Improved definition of prior uncertainties in CO2 and CO fossil fuel fluxes and its impact on multi-species inversion with GEOS-Chem (v12.5), Geoscientific Model Development, 17, 7263-7284, https://doi.org/10.5194/gmd-17-7263-2024, 2024.

Taylor, T. E., O'Dell, C. W., Baker, D., Bruegge, C., Chang, A., Chapsky, L., Chatterjee, A., Cheng, C., Chevallier, F., Crisp, D., Dang, L., Drouin, B., Eldering, A., Feng, L., Fisher, B., Fu, D., Gunson, M., Haemmerle, V., Keller, G. R., Kiel, M., Kuai, L., Kurosu, T., Lambert, A., Laughner, J., Lee, R., Liu, J., Mandrake, L., Marchetti, Y., McGarragh, G., Merrelli, A., Nelson, R. R., Osterman, G., Oyafuso, F., Palmer, P. I., Payne, V. H., Rosenberg, R., Somkuti, P., Spiers, G., To, C., Weir, B., Wennberg, P. O., Yu, S., and Zong, J.: Evaluating the consistency between OCO-2 and OCO-3 XCO2 estimates derived from the NASA ACOS version 10 retrieval algorithm, Atmos. Meas. Tech., 16, 3173-3209, 10.5194/amt-16-3173-2023, 2023.

Wang, M., Wang, S., Zhao, J., Ju, W., and Hao, Z.: Global positive gross primary productivity extremes and climate contributions during 1982-2016, Sci Total Environ, 774, 145703, https://doi.org/10.1016/j.scitotenv.2021.145703, 2021.

Whitaker, J. S. and Hamill, T. M.: Ensemble data assimilation without perturbed observations, Monthly Weather Review, 130, 1913-1924, https://doi.org/10.1175/1520-0493(2002)130<1913:EDAWPO>2.0.CO;2, 2002.

World Meteorological Organization (WMO): State of the Global Climate 2024, World Meteorological Organization, GenevaWMO-No. 1368, 2025.

Xu, J., Zhang, Z., Zhao, X., and Cheng, S.: Downward trend of NO2 in the urban areas of Beijing-Tianjin-Hebei region from 2014 to 2020: Comparison of satellite retrievals, ground observations, and emission inventories, Atmospheric Environment, 295, 119531, 10.1016/j.atmosenv.2022.119531, 2023.

Yang, H., Wu, K., Shen, H., Janssens-Maenhout, G., Crippa, M., Guizzardi, D., and Zhou, M.: A comparative analysis of China's anthropogenic CO2 emissions (2000-2023): insights from six bottom-up inventories and uncertainty assessment, Atmospheric Chemistry and Physics, 25, 18111-18127, https://doi.org/10.5194/acp-25-18111-2025, 2025.

Zhang, L., Jiang, F., He, W., Wu, M., Wang, J., Ju, W., Wang, H., Zhang, Y., Sitch, S., and Chen, J. M.: Improved estimates of net ecosystem exchanges in mega-countries using GOSAT and OCO-2 observations, Communications Earth & Environment, 5, 737, https://doi.org/10.1038/s43247-024-01910-w, 2024a.

Zhang, S., Lei, L., Sheng, M., Song, H., Li, L., Guo, K., Ma, C., Liu, L., and Zeng, Z.: Evaluating anthropogenic CO2 bottom-up emission inventories using satellite observations from GOSAT and OCO-2, Remote Sensing, 14, 5024, https://doi.org/10.3390/rs14195024, 2022.

Zhang, Z., Feng, S., Chen, Y., Liu, Q., Ju, W., Xiao, W., Huang, C., Wang, Y., Wang, H., Jia, M., Wang, X., and Jiang, F.: Development of a regional carbon assimilation system and its application for estimating fossil fuel carbon emissions in the Yangtze River Delta, China, Sci Total Environ, 957, 177720, https://doi.org/10.1016/j.scitotenv.2024.177720, 2024b.

Zhang, Z., Zhou, Y., Zhao, N., Li, H., Tohniyaz, B., Mperejekumana, P., Hong, Q., Wu, R., Li, G., Sultan, M., Zayan, A. M. I., Cao, J., Ahmad, R., and Dong, R.: Clean heating during winter season in Northern China: A review, Renewable and Sustainable Energy Reviews, 149, 111339, https://doi.org/10.1016/j.rser.2021.111339, 2021.

Zheng, B., Chevallier, F., Ciais, P., Broquet, G., Wang, Y., Lian, J., and Zhao, Y.: Observing carbon dioxide emissions over China's cities and industrial areas with the Orbiting Carbon Observatory-2, Atmospheric Chemistry and Physics, 20, 8501-8510, https://doi.org/10.5194/acp-20-8501-2020, 2020.

Zheng, B., Cheng, J., Geng, G., Wang, X., Li, M., Shi, Q., Qi, J., Lei, Y., Zhang, Q., and He, K.: Mapping anthropogenic emissions in China at 1 km spatial resolution and its application in air quality modeling, Sci Bull (Beijing), 66, 612-620, https://doi.org/10.1016/j.scib.2020.12.008, 2021.